Orbital eccentricity driven temperature variation at Mercury's poles

Matthew A. Siegler,[1,2] Bruce G. Bills,[1] and D.A. Paige[2]

Received 8 October 2012; revised 25 January 2013; accepted 8 March 2013; published 10 May 2013.

[1] Due to Mercury's extremely small obliquity, variations in orbital eccentricity are likely to have been the dominant cause of changes in polar temperatures on Mercury throughout the bulk of its history. In the last 10 Myr, the eccentricity has varied between 0.1 and 0.3. Over the past 100 Myr, eccentricity extremes of nearly zero to greater than 0.4 have likely been reached. We calculate the temperature in the near-polar region (within 10° of the North Pole) as it varies in response to past eccentricities. These calculations show periods with dramatically different temperatures, diurnal amplitudes, and long period thermal cycles—all of which can have a dramatic effect on longitudinal variations in long-term subsurface ice stability. Given forthcoming topographic data, thermal models including long-term eccentricity can help constrain when past ice might have been delivered to Mercury.

Citation: Siegler, M. A., B. G. Bills, and D. A. Paige (2013), Orbital eccentricity driven temperature variation at Mercury's poles, *J. Geophys. Res. Planets*, *118*, 930–937, doi:10.1002/jgre.20070.

1. Introduction

[2] The planet Mercury is well known for its 3:2 spin-orbit resonance (87.969 day revolution, 58.646 day spin) and eccentric orbit, $e = 0.206$ [*Colombo and Shapiro*, 1966]. The thermal effects of this spin-orbit configuration have been previously studied, showing that the eccentricity and 3:2 resonance results in a longitudinal asymmetry in temperatures [e.g., *Soter and Ulrichs*, 1967; *Paige et al.*, 1992, *Paige et al.*, 2012]. Additionally, a low obliquity (2.11 ± 1 arc min; *Margot et al.* [2007]) leads to near-polar craters with temperatures low enough to allow ice to be stable on geologic timescales [*Ingersoll et al.*, 1992; *Paige*, 1992; *Vasavada et al.*, 1999]. However, Mercury has not always been in its current orbital state.

[3] In the very distant past (likely >3.5 Gya), Mercury may not have been in the current spin-orbit resonance [*Correia and Laskar*, 2004] and likely reached higher obliquities [*Peale*, 1974; *Laskar and Robutel*, 1993; *Bills and Comstock*, 2005]. Obliquity since that time is likely to have been near to its current, Cassini State-driven value. Since this initial period, Mercury's orbital eccentricity has been both dramatically higher (up to ~0.4) and lower (down to nearly 0.0) than present [e.g., *Laskar*, 1988]. Orbital inclination also varies but is not addressed here as it does not have a direct effect on surface insolation. Therefore, we claim that over most of the past >3.5 Gyr, eccentricity variations represent the dominant change in surface insolation on Mercury. Here we aim to examine the thermal effects of those variations.

[4] The eccentricity of Mercury's orbit has likely varied from near zero to roughly 0.4 throughout its history (on the 10^9 year timescale) and at least 0.1–0.3 in the recent epoch (on the 10^7 year timescale). We examine the effects of these eccentricity variations on insolation and temperatures within 10° of the Mercurian poles. We comment on the effect these variations might have on the distribution of volatiles in near-polar craters and temperatures at depth. Volatile deposits can serve as a record of past orbital extremes, and orbital models can shed light on volatile origin. Radar observations of Mercury showed bright reflections from near-polar craters [*Slade et al.*, 1992, *Harmon and Slade*, 1992, *Harmon et al.*, 1994; *Harmon*, 2010]. These radar measurements should only be sensitive to highly concentrated (~40% by volume), nearly "clean" water ice [*Harmon et al.*, 2011]. Such pure ice may imply very recent (<50 Mya) delivery [*Crider and Killen*, 2005], warranting a detailed look at eccentricities reached during this epoch. New data from the Messenger spacecraft [*Neumann et al.*, 2012; *Lawrence et al.*, 2012; *Paige et al.*, 2012] confirms high ice concentrations and recent ice mobility. The question remains as to whether these deposits are recent or could be relics of a past epoch. Here we broadly explain the effect orbital eccentricity variations had on the past thermal environments and explore the possibility that ancient ice deposits have survived.

2. Mercury Orbit

[5] Insolation variations on Mercury are unique in the solar system. They result from the combination of high eccentricity, low obliquity, and a 3:2 spin-orbit resonance. Importantly, two longitudes (0° and 180°) alternate between being (longitudinally) subsolar during perihelion passage, causing them to receive substantially more insolation than other longitudes. *Soter and Ulrichs* [1967] labeled the

[1]Jet Propulsion Laboratory, California Institute of Technology, Pasadena, California, USA.
[2]Department of Earth and Space Sciences, University of California at Los Angeles, Los Angeles, California, USA.

Corresponding author: M. A. Siegler, Jet Propulsion Lab, University of California at Los Angeles, Los Angeles, CA, USA. (matthew.a.siegler@jpl.nasa.gov)

2169-9097/13/10.1002/jgre.20070

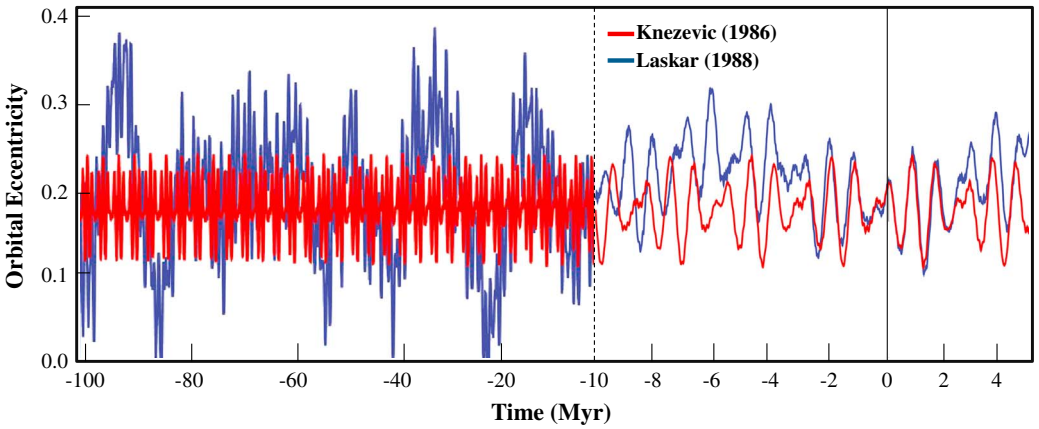

Figure 1. (in red) Secular perturbation model results for Mercury's eccentricity over the past 100 Myr from *Knezevic* [1986], which represent an update of *Brouwer and Van Woerkom* [1950]. (in blue) Semianalytic integration model results for Mercury's eccentricity over the past 100 Myr from *Laskar* [1988]. The semianalytic model, although more accurate than the secular model, should only be strictly relied upon to about −10 Myr, and model results at earlier times represent one of many possible chaotic results but show a likely range of eccentricity variation.

equatorial crossings of these longitudes "hot poles" and the equatorial longitudes at 90° and 270°, which are subsolar only at aphelion, "warm poles." We will extend these terms to imply all latitudes at longitudes 0° and 180° as "hot longitudes" and 90° and 270° as "warm longitudes" throughout this paper. The name "cold pole" is generally reserved for the latitudinal (North and South) poles. Additionally, the current eccentricity is large enough that the orbital angular velocity near perihelion exceeds the spin angular velocity, resulting in an apparent retrograde motion of the Sun when viewed from the Mercurian surface. This causes extended days along the hot longitudes, when the sun hangs in the sky near local noon, and double sunrises and sunsets along the warm longitudes [*Soter and Ulrichs*, 1967; *Cuzzi*, 1973].

[6] As eccentricity increases, the temperature difference between the warm and hot longitudes also increases. At the cold poles, the radiation pattern will become less symmetric about the rotational axis, tending to a "polar ellipse" rather than a "polar circle." The retrograde solar motion will also become more extreme with eccentricity, causing longer, warmer "retrograde days." Additionally, higher eccentricities will cause the hot longitudes to become hotter and the warm longitudes colder.

[7] The long-term eccentricity variations of Mercury have been examined using a variety of different models, including analytical secular perturbation models [i.e., *Brouwer and Clemence*, 1946; *Brouwer and Van Woerkom*, 1950; *Bretagnon*, 1984; *Laskar*, 1984a, 1984b; *Knezevic*, 1986; *Boccaletti and Pucacco*, 1998] and numerical integrations [i.e., *Laskar*, 1988; *Sussman and Wisdom*, 1992; *Laskar*, 1994; *Ito and Tanikawa*, 2002; *Correia and Laskar*, 2004]. Several general features emerge from these studies. Most important for the present discussion are large, nearly periodic oscillations in eccentricity, mainly due to secular perturbations from Venus and a lesser extent from Earth and Mars [*Brouwer and Van Woerkom*, 1950; *Murray and Dermott*, 1999]. Over the past few million years, most models agree, in a general sense, with the secular perturbation theory of *Brouwer and Van Woerkom* [1950] and its minor corrections by *Knezevic* [1986] but show that this solution should only be considered a first-order approximation. These calculations result in quasi-periodic (~1 Myr period) oscillations in eccentricity between approximately 0.1 and 0.3.

[8] For timescales longer than a few million years, numerical integration reveals limits of the secular theory. *Laskar* [1988] used a semianalytic method using a secular model for short, orbital time periods, combined with numerical integrations over longer timescales. This system has been validated with comparison with direct integration, as in *Correia and Laskar et al.* [2004], and reveals the importance of chaotic behavior in determining orbital elements in the distant past. As the results are inherently chaotic, exact values of eccentricity are difficult to predict, but repeated integrations can reveal statistical likelihoods of a given eccentricity. These models predict likely 100 Myr timescale variations from approximately zero to 0.4 eccentricity [e.g., *Laskar*, 1988; *Correia and Laskar*, 2004].

[9] It is clear that the orbital eccentricity of Mercury does exhibit large oscillations. Given an early tidal damping of Mercury's obliquity [*Correia and Laskar*, 2004] and lack of resonant forcing [*Peale*, 1974, 2006] or evidence of impacts [*Correia and Laskar*, 2012] available to increase obliquity once damped, eccentricity variations should have the largest influence on near-surface temperatures out of any events in the past several billion years. Here we seek to understand the thermal implications of those variations. Figure 1 illustrates the result from a secular perturbation model (*Knezevic* [1986]—which is an update of *Brouwer and van Woerkom* [1950]) in red and a result of an example, long-term, semianalytic integration [*Laskar*, 1988] in blue. The semianalytic model, although more accurate than the secular model, should only be strictly relied upon to about −10 Myr, and model results at earlier times represent one

of many possible, chaotic results but show a likely range of eccentricity variation.

[10] In summary, we assume the recent dynamics (in the past ~10 Myr) of Mercury to be defined by a 3:2 spin-orbit resonance, with zero obliquity and a semiperiodic variation in eccentricity between 0.1 and 0.3, so we choose to model these eccentricities to represent this recent 10 Myr. If delivery of ice is truly recent [*Crider and Killen*, 2005], this period may dominate the distribution of ice. Earlier than that time, nearly circular orbits (0 eccentricity) and eccentricities exceeding 0.325 and reaching as high as 0.425 are likely to have occurred [*Correia and Laskar*, 2004]. This has been the largest variation to Mercury's insolation since a capture into a 3:2 resonance and Mercury's spin pole was driven into a low obliquity Cassini State, likely shortly after the Caloris Basin impact formed (~3.7 Gya, *Le Feuvre and Wieczorek* [2011]; *Correia and Laskar* [2012]). To represent this long-term period, we model eccentricity values of 0 to 0.4. If volatile distributions retain some correspondence to these extremes, it may imply an ancient origin. We briefly address the impact this would have on volatile stability on Mercury, which is primarily left for future work.

3. Thermal History

[11] The calculation of surface temperatures of Mercury began shortly after the determination of the 3:2 spin-orbit resonance by *Colombo* [1965]. Notable models were presented by *Soter and Ulrichs* [1967], *Morrison* [1968, 1970], *Cuzzi* [1973], *Paige et al.* [1992], and *Mitchell and de Pater* [1994], all with increasing complexity in subsurface thermal properties. Here we adopt the subsurface thermal model of *Vasavada et al.* [1999], which treats the subsurface as a porous regolith (1800 kg m^{-3}) with an overlying 2 cm-thick extremely porous layer (1300 kg m^{-3}). This simplified model has been shown to be consistent with radar observations of Mercury [*Mitchell and de Pater*, 1994] and surface and subsurface temperatures on the Moon [*Vasavada et al.*, 1999, *Vasavada et al.*, 2012]. This paper will focus on temperatures in the region lying within 10° of latitude of the cold poles, where near-surface ice is most likely to exist.

[12] Figure 2 illustrates calculated current temperatures in the polar region (similar to *Paige* [1992]) for a spherical planet with a noncratered surface. As Mercury has negligible obliquity, and is assumed zero here, these results correspond to either pole. Each quadrant is a map of 70 separate one-dimensional thermal models spaced every 1° in latitude and 11.25° in longitude. Maximum, minimum, and average temperature values are taken over a biannual (two Mercury-year) period, which represents one complete insolation cycle. White lines mark latitude in 2° steps (80°, 82°, 84°, 86°, and 88°); contour intervals are 2 K (for minimum), 10 K (for mean), and 20 K (for maximum), respectively. These models use the same conditions as *Vasavada et al.* [1999], including one-dimensional, plane-parallel, thermal model with the two-layered thermal properties, 95% emissivity, 0.1 albedo, and 33 mW m^{-2} lower boundary heat flux (see more details in Appendix A).

[13] Several first-order patterns emerge. Biannual minimum (Figure 2a) and mean (Figure 2b) temperatures display an imprint of the longitudinal asymmetry in insolation,

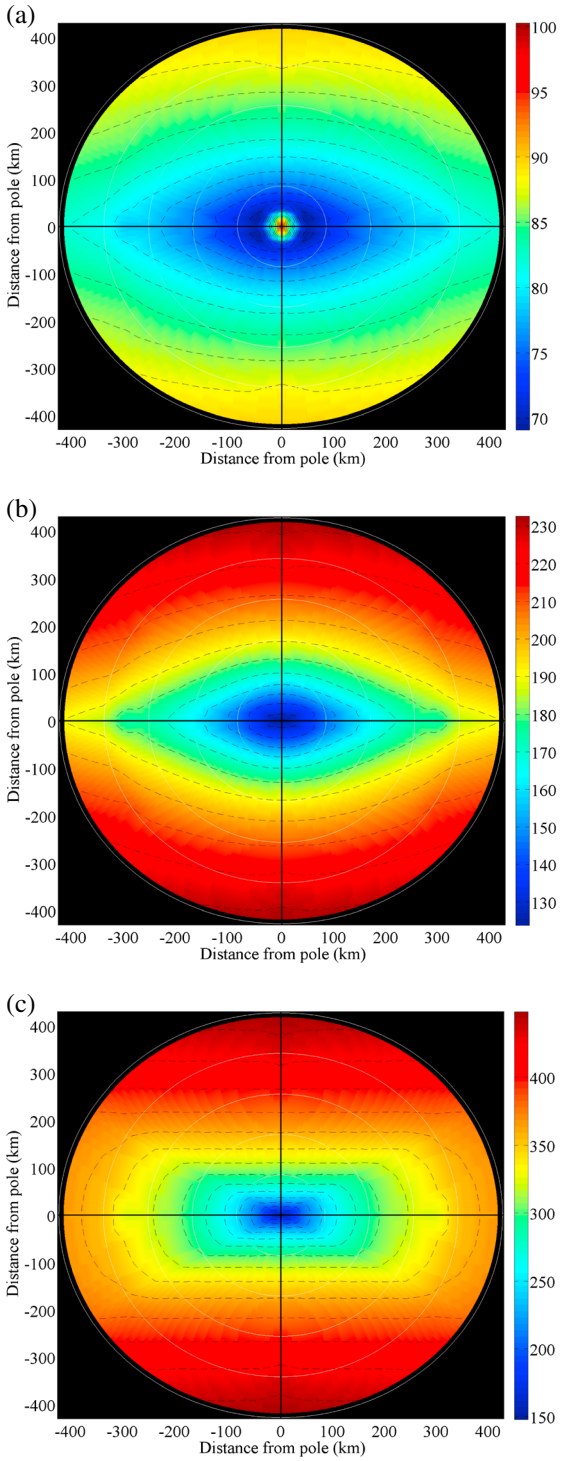

Figure 2. Modeled current polar temperatures of a crater-free Mercury: Biannual (a) minimum, (b) mean, and (c) maximum. White lines mark 80°, 82°, 84°, 86°, and 88° latitude; 0° longitude is at the bottom. Contour intervals are at 2, 10, and 20 K, respectively.

resulting in warmer temperatures along the hot longitudes due to the resonant perihelion passage. A curious rise in minimum temperature near the cold pole is due to continuous partial nighttime illumination caused by the finite size of the solar disk (approximately 2° in the Mercurian sky). The rectangular shape of the contours of maximum

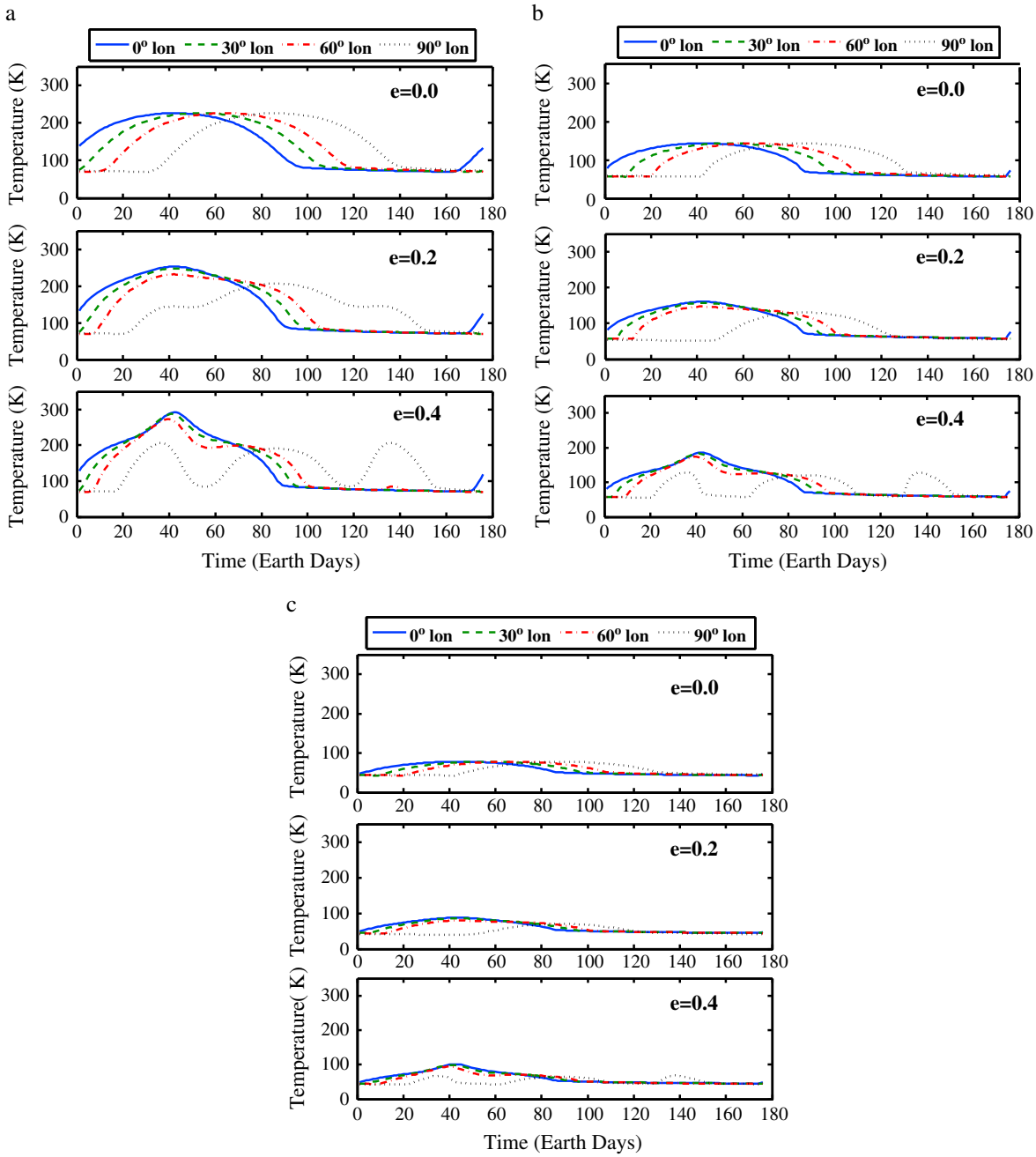

Figure 3. Temperatures on (a) a flat surface or (b) 1:5 and (c) 1:16 depth-to-diameter ratio craters at 89° latitude for Mercury at 0.0, 0.2 (current), and 0.4 eccentricity.

(Figure 2c) temperature can be thought of as a "burnt in" impression of the two hottest days of the year when Mercury is at perihelion, which form the long sides of the rectangle, and the impression of the noontime illumination of the warm longitudes at aphelion forming the short sides.

[14] The central aim of this paper is to understand how temperatures should vary in Mercury's polar environment in response to eccentricity changes. Figure 3a illustrates the change in the biannual surface temperature at 89° latitude on Mercury due to eccentricity changes. Note the growth of importance of the "retrograde days" (at ~days 35 and 135) with increasing eccentricity, especially at 90° (and 270°) longitude. At 0.4 eccentricity, a large peak (292 K in this model) also grows at 0° (and 180°) longitude at local "noon." To put the extremes experienced at this eccentricity in perspective, running this model at the equator, not shown here, shows that this peak reaches 805 K midday and dips to 111 K at night for a flat surface.

[15] Additionally, we would like to examine temperatures within shadowed craters, as these are the areas most likely to harbor ice. We chose to model craters assuming a spherical section (as in *Ingersoll et al.* [1992]) with depth-to-diameter ratios of either 1:5 or 1:16. These were chosen to represent craters of less than ~10 and between ~10 and 25 km diameter, respectively [*Pike*, 1974, 1977; *Paige*, 1992]. A cratered surface will diminish temperature

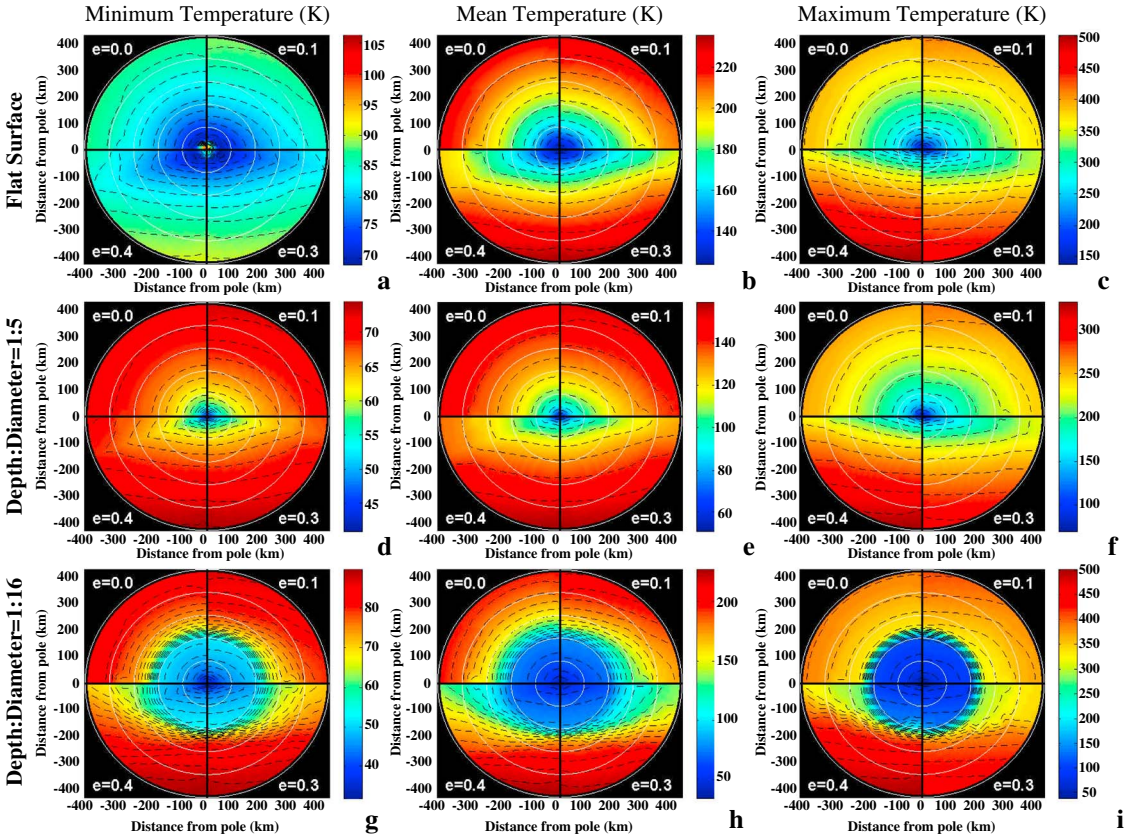

Figure 4. Modeled minimum, mean, and maximum temperature results for Mercury at various eccentricities for a crater-free surface, one covered by craters with 1:5 depth-to-diameter ratio and one covered by craters with 1:16 depth-to-diameter ratio. As obliquity is zero, all four quadrants about the pole can be mirrored, allowing us to plot only one example quadrant at each eccentricity. White lines mark 80°, 82°, 84°, 86°, and 88° latitude; 0° longitude is at the bottom.

variations, as crater floors are illuminated only by reflected light from the partially illuminated crater walls and reradiated infrared light from the entire crater (calculated here as described in *Siegler et al*. [2011] and *Ingersoll et al*. [1992]). The representation of a crater as a spherical section allows for an analytical insolation function, as radiation is scattered equally to all surfaces within the crater [*Siegler et al*., 2011]. All our model results are for a point at the center of such a crater. Figures 3b and 3c show polar temperatures within (at the center of the floor) a crater placed at the same 89° latitude.

[16] As an example, at 0.4 eccentricity, the peak temperature in a crater with a depth-to-diameter ratio of 1:5 will drop to 186 K; for 1:16, 101 K. Minimum temperatures also drop (71 K for a flat surface, 58 K for 1:5, and 45 K for 1:16 at 0.4 eccentricity), as do mean (143 K for a flat surface, 98 K for 1:5, and 61 K for 1:16 at 0.4 eccentricity). Temperatures at depth are approximated by the mean temperature (actual modeled temperatures at 1 m depth are 153, 103, and 65 K, namely due to geothermal heat and temperature-dependent thermal properties).

[17] We can expand this analysis by mapping temperatures for a crater floor placed at any location. Although some knowledge of actual crater size and location does exist [e.g., *Vasavada et al*., 1999; *Harmon*, 2010], and high resolution topography will soon be available (Mercury Laser Altimeter instrument aboard the MESSENGER spacecraft; *Cavanaugh et al*. [2007]; *Neumann et al*. [2012]), here we wish to examine the theoretical spatial effect of eccentricity changes, placing an identical cratered terrain at every point on the map. This will reveal if there are any expected longitudinal trends in temperature conditions conducive to ice retention. Figure 4 attempts to compile all of these variations.

[18] Figures 4a–4c illustrate the same quantities as shown in Figure 2 but at various eccentricities. Taking advantage of the symmetry that results from Mercury's ~0° obliquity and 3:2 spin-orbit resonance, we only need one quadrant to illustrate the effects over the entire polar region (which can simply be mirrored about 0° and 90° longitude), so four representative eccentricities can be plotted at once.

[19] Figures 4a–4c show the effect of eccentricity changes (0.0, 0.1, 0.3, and 0.4 eccentricity) on the modeled temperatures presented in Figure 2. The essential feature is an oscillation of the ellipticity of temperature contours about the pole, from circular at $e = 0.0$ to highly elongated at $e = 0.4$. The $e = 0.0$ case illustrates that the 3:2 spin-orbit resonance alone produces no effect on longitudinal surface temperature distribution but only serves to localize effects of eccentricity (which would itself have no impact for a fast rotator). Only in the unique combination that occurs on Mercury will this "polar ellipse" occur. This effect becomes more extreme at 0.4 eccentricity, where temperatures dramatically increase

along 0°/180° (hot longitudes) but decrease along 90°/270° (warm longitudes).

[20] A flat surface is not likely to promote long-term ice stability (1 m of ice will be lost in a billion years at ~100 K; e.g., *Siegler et al*. [2011]) as all modeled mean temperatures exceed roughly 130 K. However, as illustrated in Figures 4d–4f, temperatures in a crater with 1:5 depth-to-diameter ratio are such that it may be able to harbor ice. If the surface were covered with craters, one could imagine that the distribution of ice might expand along the 90°/270° axis and contract along the 0°/180° axis. Figures 4d and 4e show that as eccentricity decreases, warmer temperatures reach to higher latitudes. This can also be seen in maximum temperatures (Figure 4f), where relatively low temperatures extend further equatorward during high eccentricities. So, somewhat counter intuitively, when eccentricities are high and perihelion is closer to the Sun, ice actually has a greater area over which it might be stable. Despite the change in orbital radius, mean temperatures do not vary dramatically at the hot longitudes. The most extreme changes occur at the warm longitudes.

[21] In the case of shallower 1:16 depth-to-diameter craters (Figures 4g–4i), the drop in temperatures is even more extreme. However, equatorward of ~86° latitude, light will shine over the crater wall, illuminating the floor, actually causing it to be slightly warmer than a flat surface (due to radiation off of the crater wall). This leads to a sharp latitudinal boundary at which crater floors will suddenly become illuminated (at latitude = tan[depth/diameter], so this same transition happens at ~78° latitude for 1:5 depth-to-diameter). However, note that this model does not account for sloped crater walls. This boundary varies little with eccentricity, changing only slightly due to the apparent angular diameter of the Sun. Small craters containing ice outside these boundaries (as have been seen in the radar data sets down to as low as 67° latitude along ~60° W longitude; *Harmon* [2010]) imply either large-scale topography underlying these craters (which could preferentially tilt them poleward as in the case of the newly discovered "Northern Rise" along that longitude) or very young, mobile ice. These low-latitude craters would be especially susceptible to changes in eccentricity and might be used to date recent ice delivery or mark recent redistribution.

4. Implications for Ice Stability and Mobility

[22] It is important to note that any true model of volatile stability and mobility requires a model of supply. In the case of Mercury, the present supply of water molecules, or even solar wind hydrogen, which may lead to water formation [e.g., *Crider and Vondrak*, 2003], is highly uncertain. Extrapolating the rate of volatile delivery into the distant past would be even more speculative. Additionally, this paper is aimed to examine the theoretical spatial variations in the thermal environment rather than use a detailed topographic thermal and volatile mobility model [e.g., *Paige et al*., 2012]. In light of these constraints, we can only focus on thermal effects on ice stability and mobility that should be independent of supply as a basis for future work based on new topography measurements.

[23] *Paige* [1992] illustrated current temperatures of a flat surface near the North and South poles of Mercury, showing that the inclusion of a simple cratered terrain would lead to areas where ice could be stable even with no supply (their stability criteria was a time-averaged loss rate less than 1 kg m^{-2} Gyr^{-1} for exposed water ice, which occurs at ~100 K). Using Figures 4c, 4f, and 4i, it is apparent that, at all modeled eccentricities, surface ice should only be expected at latitudes above approximately 88° in craters with depth-to-diameter ratios shallower than 1:16, which appears to be consistent with radar observations [*Harmon*, 2010].

[24] This is only part of the story. At slightly higher temperatures (~100–130 K), ice can be stable if buried [e.g., *Paige et al*., 2010; *Paige et al*., 2012]. In this temperature range, ice will also be mobile enough to redistribute itself [*Schorghofer and Taylor*, 2007; *Siegler et al*., 2011]. Areas with larger thermal gradients (higher yearly maximum temperatures that stay below ~130 K, when ice is generally unstable in the top several meters; *Paige et al*. [2010]) could feasibly have mobile ground ice, migrating at a rate determined by the thermal gradient, which varies with depth [e.g., *Schorghofer*, 2010].

[25] Long-term variations will also affect subsurface ice. A dry regolith layer above subsurface ice will serve both to diminish the maximum temperature felt at depth and to inhibit upward diffusion of volatiles. If an overlying layer is entirely ice free, temperatures will damp to approximately the mean temperature (see Figures 4b, 4e, and 4h) by ~1.5 m depth. At certain longitudes (roughly along 90°/270° longitude line), the change in mean temperature due to eccentricity can be up to 30 K for a flat surface, 25 K for a 1:5 depth-to-diameter ratio, and nearly 45 K for a 1:16 depth-to-diameter ratio. As these changes happen over long periods of time (10^5–10^6 years, see Figure 1), these differences in mean temperature would imply similar amplitude changes in temperatures at depths of tens of meters.

5. Conclusions

[26] The high-latitude regions of Mercury have gone through substantial changes in temperature over the course of the last 4 Gyr. These changes are primarily due to eccentricity variations. The thermal effects of the eccentricity oscillations, with 10^5–10^6 year period [*Brouwer and Van Woerkom* 1950], are large enough that they need to be taken into account when modeling long-term ice stability.

[27] Maximum temperatures over much of the region poleward of 80° can vary by up to 80 K on a flat surface or about 45 K in a crater (with a 1:5 depth-to-diameter ratio) over the past few 10^7 years, causing extreme changes in surface volatile stability. Mean temperatures can vary by 30 K on a flat surface and up to 45 K in a crater (with a 1:16 depth-to-diameter ratio), implying large temperature changes at depth. Ice buried below a protective layer of regolith, which will both diminish the maximum temperature and cause a barrier to outward vapor diffusion, may be able to survive at greater temperatures. If locations found to contain ground ice today were highly unstable in a past eccentricity, this may argue for recent (in the past 10^7 years) deposition of ice.

[28] If thermal environments in radar bright areas are stable for water ice at all eccentricities experienced, it may imply that the ice deposits of Mercury are very old (likely as old as the Caloris basin impact ~3.7 Gya). However, this would require a mechanism to allow ice to be mobile enough to form coherent blocks, despite impact gardening. We are

not aware of any laboratory experiment that has shown an ability to make nearly pure ice by migration of water vapor through regolith, especially at temperatures below 150 K. The same questions and laboratory work that are being applied to nearly pure ground ice formation on Mars may also be applicable here and might prove fruitful for future research. If pure ice cannot be formed by redistribution of buried deposits, this implies that the radar coherent deposits on Mercury are indeed young (less than 50 Myr; *Crider and Killen* [2005]; *Hurley et al*. [2012]). This could be confirmed by observation of ice in craters that were unstable at 0.35–0.4 eccentricity, which would also imply a ~50 Myr upper limit age.

Appendix A: Mercury Orbit and Thermal Model Details

[29] The solar radiation, incident upon the surface of a spherical planet (as is assumed in this paper), can be written as

$$F = \frac{S}{r^2} \| \cos[\gamma] \|, \tag{A1}$$

where $S = 1370\ \mathrm{W/m^2}$ is the solar flux at 1 AU, r is the distance from the Sun (in AU), γ is the solar zenith angle or angular separation between local zenith and direction to the Sun, and the clipping operator is

$$\| x \| = \frac{x + |x|}{2}. \tag{A2}$$

[30] This expression yields x if x is nonnegative and yields 0 otherwise. For times when the solar disk (which measures roughly 2° in the Mercurian sky) is partially obscured, $\| \cos[\gamma] \|$ from equation (A1) reverts to the more general $\cos[\gamma]$, and S is scaled by the portion of the solar disk exposed above the horizon (similar to *Cuzzi* [1973]). Our model also includes a value of solar limb darkening as found in *Negi et al*. [1985].

[31] On a surface with albedo A, the absorbed radiation is

$$Q = (1 - A)F = (1 - A)\frac{S}{r^2} \| \cos[\gamma] \|. \tag{A3}$$

[32] Our thermal model thus needs to compute the temporal variations in solar zenith angle γ, at each point, and temporal variations in solar distance r.

[33] In a binary orbit, the distance varies according to

$$r = a\left(\frac{1 - e^2}{1 + e\cos[f]}\right), \tag{A4}$$

where a is semimajor axis, e is eccentricity, and f is true anomaly or angular distance from periapse.

[34] At a point with coordinates {latitude,longitude} = $\{\theta,\phi\}$ and a time when the subsolar point is at location $\{\theta_s,\phi_s\}$, the solar zenith angle is given by

$$\cos[\gamma] = \sin[\theta]\sin[\theta_s] + \cos[\theta]\cos[\theta_s]\cos[\phi - \phi_s]. \tag{A5}$$

[35] Since the obliquity of Mercury is very small, we can take $\theta_s = 0$, and due to the 3:2 spin-orbit resonance, the subsolar longitude varies with time according to

$$\phi_s = \frac{3}{2}M - f, \tag{A6}$$

where M is mean anomaly and f is true anomaly. The mean anomaly varies linearly with time, according to

$$\frac{dM}{dt} = n, \tag{A7}$$

where n is mean motion. True anomaly has a nonlinear variation with time but is related to mean anomaly via Kepler's second law, which is

$$r^2\frac{df}{dt} = a^2\sqrt{1 - e^2}\frac{dM}{dt}. \tag{A8}$$

[36] A common strategy for computing true anomaly as a function of time is to use the intermediate variable eccentric anomaly E, which is related to mean anomaly via Kepler's equation

$$M = E - e\sin[E], \tag{A9}$$

and is also related to true anomaly via

$$\tan\left[\frac{f}{2}\right] = \sqrt{\frac{1 + e}{1 - e}}\tan\left[\frac{E}{2}\right]. \tag{A10}$$

[37] Kepler's equation can be solved iteratively via the Newton-Raphson method,

$$E_1 = M \tag{A11}$$

$$E_{j+1} = E_j + \frac{M + e\sin[E_j] - E_j}{1 - e\cos[E_j]} \tag{A12}$$

[38] This converges quadratically in eccentricity, and the third term is thus accurate to order e^6.

[39] Time-varying temperatures as a result of this surface flux are then calculated using a layered numerical thermal model. Most of the details behind this thermal model have been presented in *Siegler et al*. [2011], including a model to calculate temperatures at the center of a bowl-shaped crater (that is a section of a sphere). *Vasavada et al*. [1999] details the regolith thermal and density structure (with a 2 cm upper layer, density $1300\ \mathrm{kg\,m^{-3}}$, $k_c = 9.22 \times 10^{-4}$, $\chi = 1.48$, and lower layer, density $1300\ \mathrm{kg\,m^{-3}}$, $k_c = 9.3 \times 10^{-3}$, $\chi = 0.073$, where thermal conductivity $k = k_c\left(1 + \chi\left(\frac{T}{350}\right)^3\right)$) is assumed in the current paper, with modifications of the albedo (assumed 0.1) and heat flux (assumed $33\ \mathrm{mW\,m^{-2}}$). A slightly revised regolith model has been developed for the Moon and may also be appropriate for Mercury but would have only a minor impact on results presented here [*Vasavada et al*., 2012]. Timesteps were typically 300 s with 400+ layers, each 5 mm thick. Models were

run from a fixed initial temperature (typically 100 K) for >50 Earth years (~200 Mercury orbits) to assure thermal equilibrium had been reached.

[40] **Acknowledgments.** Thank you to Jean-Luc Margot, David Jewitt, Dana Hurley, Ashwin Vasavada, and Jean-Pierre Williams for useful discussions. Thank you to Sue Smrekar for the patience as I finished another fraction of my thesis. Part of the research was carried out at the Jet Propulsion Laboratory, California Institute of Technology, under a contract with the National Aeronautics and Space Administration.

References

Bills, B. G., and R. L. Comstock (2005), Forced obliquity variations of Mercury, *J. Geophys. Res.*, *110*, E04006.

Boccaletti, D., and G. Pucacco (1998), *Chaos in N-body systems Planetary and Space Science*, *46*, 1557–1566. doi:10.1016/S0032-0633(97)00214-6.

Bretagnon, P. (1984), Improvement of analytical planetary theory, *Celest. Mech.*, *34*, 193–201, doi:10.1007/BF01235801.

Brouwer, D., and G. M. Clemence (1946), Numerical development of the disturbing function by correction of an approximate development, *Astron. Jour.*, *52*,64–67, doi:10.1086/105915 Published: 1946.

Brouwer, D., and A. J. J. van Woerkom (1950), Astron. Papers Amer. Eph. 13, Pt. 2, 81–10.

Cavanaugh J. F., et al. (2007) The Mercury laser altimeter instrument for the MESSENGER mission space science reviews V. 131, Numbers 1–4, 451–479, doi:10.1007/s11214-007-9273-4.

Colombo, G. (1965), Rotational period of planet Mercury, *Nature*, *208*, 575. doi:10.1038/208575a0.

Colombo, G., and I. I. Shapiro (1966), Rotation of planet Mercury, *Astrophys. J.*, *145*, 296, doi:10.1086/148762.

Correia, A. C. M., and J. Laskar (2004), Mercury's capture into the 3/2 spin-orbit resonance as a result of its chaotic dynamics, *Nature*, *429*.

Correia, A. C. M., and J. Laskar (2012), Impact cratering on Mercury: Consequences for the spin evolution, *Astrophys. Jour. Lett.*, *751*:L43, doi:10.1088/2041-8205/751/2/L43.

Crider, D. H., and R. R. Vondrak (2003), Space weathering of ice layers in lunar cold traps, *Adv. Space Res.*, *31*(11), 2293–2298.

Crider, D. H., and R. Killen (2005), Burial rate of Mercury's polar volatile deposits, *Geophys. Res. Letters*, *32*, L12201, doi:10.1029/2005GL022689.

Cuzzi, J. N. (1973), The subsurface nature of Mercury and Mars from thermal microwave emission. *PhD Thesis*, California Institute of Technology.

Harmon, J. K., and M. A. Slade (1992), Radar mapping of Mercury: Full-disk images and polar anomalies, *Science*, *258*, 640–643.

Harmon, J. K., M. A. Slade, R. A. Velez, A. Crespo, M. J. Dryer, and J. M. Johnson (1994), Radar mapping of Mercury's polar anomalies, *Nature*, *369*, 213–215.

Harmon, J., M. Slade, and M. Rice (2011), Radar imagery of Mercury's putative polar ice: 1999–2005 Arecibo results, *Icarus*, *211*(1), 14.

Hurley, D. M., D. J. Lawrence, B. J. Bussey, R. R. Vondrak, R. C. Elphic, and G. R. Gladstone (2012), Two-dimensional distribution of volatiles in the lunar regolith from space weathering simulations, *GRL*, *39*, L09203, 6 PP., 2012, doi:10.1029/2012GL051105.

Ingersoll, A. P., T. Svitek, and B. Murray (1992), Stability of polar frosts in spherical bowl-shaped craters on the Moon, *Mercury, and Mars, Icarus*, *100*, 40–47.

Ito, T., and K. Tanikawa (2002), Long-term integrations and stability of planetary orbits in our Solar system, *Mon. Not. R. Astron. Soc.*, *336*, doi:10.1046/j.1365-8711.2002.05765.X.

Knezevic, Z. (1986), Secular variations of major planets orbital elements, *Celest. Mech.*, *38*, 123–138, doi:10.1007/BF01230425.

Laskar, J. (1984a), Théorie Générale Planétaire. Eléments orbitaux des planètes sur 1 million d'années. PhD Thesis, IMCCE - Institut de Mécanique Céleste et de Calcul des Ephémérides

Laskar, J. (1984b), Progress in general planetary theory, *Celest. Mech.*, *34*, p219–221, doi:10.1007/BF01235803.

Laskar, J. (1988), Secular evolution of the solar system over 10 million years, *Astron. Astrophys.*, *198*, 341–362.

Laskar, J. (1994), Large-scale chaos in the Solar System, *Astron. Astrophys.*, *287*, L9–L12.

Laskar, J., and P. Robutel (1993), The chaotic obliquity of the planets. *Nature*, *361*, 608–612, doi:10.1038/361608a0.

Lawrence, D. J. et al. (2012), Evidence for water ice near Mercury's north pole from MESSENGER neutron spectrometer measurements, *Science*, doi:10.1126/science.1231106.

Le Feuvre, M., and M. A. Wieczorek (2011), Nonuniform cratering of the Moon and a revised crater chronology of the inner Solar System, *Icarus*, *214*.

Margot, J. L., S. J. Peale, R. F. Jurgens, M. A. Slade, and I. V. Holin (2007), Large longitude libration of Mercury reveals a molten core, *Science*, *316*, doi:10.1126/science.1140514.

Mitchell, D. L., and I. de Pater (1994), Microwave imaging of Mercury's thermal emission at wavelengths from 0.3-cm to 20.5-cm, *Icarus*, *110*, 2–32, doi:10.1006/icar.1994.1105.

Morrison, D. (1968), Thermal models and microwave temperatures of the planet Mercury. SAO Special Report #292.

Morrison, D. (1970), Thermophysics of the planet Mercury, *Space Sci. Rev.*, *11*, 271.

Murray, C. D., and S. F. Dermott (1999), *Solar System Dynamics*, Cambridge University Press, Cambridge, U.K.

Negi, B. S., N. C., Bhowmik, S. S. Mathur, and T. C. Kandpal (2005), Solar limb darkening and ray trace evaluation of solar concentrators, *Applied Optics*, *24*(2), 296–298.

Neumann, G. A. et al. (2012), Bright and dark polar deposits on Mercury: Evidence for surface volatiles, *Science*, doi:10.1126/science.1229764.

Paige, D. A. (1992), The thermal stability of near-surface ground ice on Mars, *Nature*, *356*, 43–45.

Paige, D. A., S. E. Wood, and A. R. Vasavada (1992), The thermal stability of ice at the poles of Mercury, *Science*, *258*, 5082, 643–646.

Paige, D. A., M. A. Siegler, J. K. Harmon, G. A. Neumann, E. M. Mazarico, D. E. Smith, M. T. Zuber, E. Harju, M. L. Delitsky, and S. C. Solomon (2012), Thermal stability of volatiles in the north polar region of Mercury, *Science*, doi:10.1126/science.1231106.

Paige, D. A. et al. (2010), Diviner observations of cold traps in the lunar south polar region: Spatial distribution and temperature, *Science*, *330*.

Peale, S. J. (1974), Possible histories of obliquity of Mercury, *Astron. J.*, *79*, 722–744, doi:10.1086/111604.

Peale, S. J. (2006), The proximity of Mercury's spin to Cassini state 1 from adiabatic invariance, *Icarus*, *181*.

Pike, R. J. (1974), Depth/diameter relations of fresh lunar craters: Revision from spacecraft data, *Geophys. Res. Lett.*, *1*, 291–294.

Pike, R. J. (1977), Apparent depth/apparent diameter relation for lunar craters, Proceedings of the 8th Lunar Science Conference, 3427-3436.

Schorghofer, N. (2010), Fast numerical method for growth and retreat of subsurface ice on Mars, *Icarus*, *208*, 598–607.

Schorghofer, N., and G. J. Taylor (2007), Subsurface migration of H_2O at the lunar poles, *J. Geophys. Res.*, *112*, E02010.

Siegler, M. A., B. G. Bills, D. A. Paige (2011), Effects of orbital evolution on lunar ice stability, *JGR Planets*, *116*, E03010, doi:10.1029/2010JE003652.

Slade, M. J., B. J. Butler, and D. O. Muhleman (1992), Mercury radar imaging: Evidence for polar ice, *Science*, *258*, 635–640.

Soter, S., and J. Ulrichs (1967), Rotation and heating of planet Mercury, *Nature*, *214*, 1315, doi:10.1038/2141315a0.

Sussman, G. L., and J. Wisdom (1992), Chaotic evolution of the solar-system, *Science*, *257*, 56–62, doi:10.1126/science.257.5066.56.

Vasavada, A. R., L. Bandfield, B. Greenhagen, P. Hayne, M. Siegler, Williams J., and Paige, D. (2012), Lunar equatorial surface temperatures and regolith properties from the Diviner Lunar Radiometer Experiment—JGR in press.

Vasavada, A. R., D. A. Paige, and S. E. Wood (1999), Near-surface temperatures on Mercury and the Moon and the stability of polar ice deposits, *Icarus*, *141*, 179–193.